Int. J. Electrochem. Sci., 15 **(2020)** 6706 – 6716, doi: 10.20964/2020.07.26

International Journal of
ELECTROCHEMICAL
SCIENCE
www.electrochemsci.org

Preparation and Bacterial Adsorption Behaviors of Zeolite-Modified Anode in Microbial Fuel Cells

Fei Tong[1], *Jie Gong*[1], *Jinlong Jiang*[2,*], *Lixiong Zhang*[3,*] *and Xiayuan Wu*[3]

[1] Key Laboratory of Precious Metal Chemistry and Technology of Jiangsu Province, Jiangsu University of Technology, Changzhou 213001, PR China
[2] Jiangsu Provincial Key Laboratory of Palygorskite Science and Applied Technology, Huaiyin Institute of Technology, Huai'an 223003, PR China
[3] State Key Laboratory of Materials-Oriented Chemical Engineering, College of Chemistry and Chemical Engineering, Nanjing Tech University, No. 5 Xin Mofan Rd., Nanjing 210009, PR China
[*]E-mail: jljiang@hyit.edu.cn, lixzhang@njtech.edu.cn

Received: 2 March 2020 / *Accepted:* 14 April 2020 / *Published:* 10 June 2020

A zeolite-modified graphite anode was prepared by an in-situ hydrothermal method combined with acid pretreatment, and it showed higher output voltage in dual-chamber microbial fuel cells (MFCs) than the bare graphite felt anode (630.4 vs. 524.6 mV). The anode was modified with different types of zeolite by changing the zeolite synthesis conditions, which was characterized by XRD and SEM to examine the type of modified zeolite on anode, and the modification with NaX zeolite outperformed NaA zeolite. Dispersion of more zeolite on the graphite felt was also an important effect to improve the MFC performance. After examing the effect of zeolite on bacterial adsorption was examined, it was found that the wetting and glucose adsorption abilities of the anode were greatly improved by zeolite modification and enabled the anode to attach more bacterial cells. Large amount of agglomerated crystals cannot provide suitable environment for microbial growth, so the zeolite should be dispersed.

Keywords: Zeolite; Microbial fuel cells; Anode modification; bacterial adsorption

1. INTRODUCTION

Microbial fuel cells (MFCs) utilize bacteria as the catalysts to oxidize organic (inorganic) matter, converting chemical energy into electricity directly via electricigens, and can be potentially applied into environmental pollution treatment and energy storage [1]. Despite their advantages, the application of MFCs is limited by low power generation efficiency and high cost [2-3], which make it necessary to improve the power output of MFCs. Traditional MFCs are composed of an anode chamber and a cathode chamber separated by an ion-exchange membrane. The anode material plays an important role in the MFC performance because it acts as a bacterial carrier and an electron collector [4-5]. An ideal anode

material should possess low resistance, high electrical conductivity, strong biocompatibility, large surface area and chemical stability [6]. Traditional anodes are made of carbon-based materials, including graphite felt, graphite brush, and graphite cloth [7]. Nowadays, researchers pay attention to the modification of carbon-based anodes because the physiochemical properties are changed for better microbial attachment and electron transfer.

So far, the MFC modification methods mainly include heat modification and acid modification. For instance, carbon brush heatment in a muffle furnace at 450 ^{o}C for 30 min enlarged the anode surface area from 7.11 to 49.3 m^2/g and maximized power density to 1.28 W/m^2 [8]. The methane acid pretreatment of carbon cloth anode increased the power density from 5.2 to 28 [9]. These methods can remove impurities efficiently and enlarge the active surface area and conductivity, but not significantly. Chemical modification, which is effective for immobilizing metals, metal oxides or other active compounds on the carriers, can obviously enhance the output power. Zhang' group modified the anode with carbon nanotubes, and the current density, power density and coulombic efficiency are increased by 46.2%, 58.8% and 84.6%, respectively [10]. Based on the report from Li, the carbon cloth anode were treated with HNO_3, H_2SO_4, NH_4NO_3 or $(NH_4)_2SO_4$ and improved the power density in all cases [11]. Moreover, the combination of some anode modification methods can improve the performance of MFCs [12-14].

Zeolites are widely used in the fields of separation, purification and catalysis industry thanks to their unique pore size, large surface area and high thermal stability [15-17]. In our premier work, zeolite MCM-41 and NaX were successfully coated on graphite felt by an in-situ hydrothermal method [1, 18]. In this essay, the graphite felt anode was modified with different types of zeolite after acid pretreatment. The electrochemical capability of anodic biofilm of anodes was also characterized by cyclic voltammetry (CV). We investigated the effects of modification parameters on MFC power and discussed the principle.

2. EXPERIMENTAL

2.1 Methods

The bare graphite felt (5.0 × 5.0 × 0.5 cm^3; Hunan Jiuhua Carbon Hi-Tech Co., Ltd., China) was firstly dipped in a 10 wt% HNO_3 solution (Shanghai Lingfeng Chemical Reagent Co. Ltd.) at a 90 ^{o}C oven. After 3 h of acid treatment, the graphite felt was taken out and washed with deionized water for several times. Then it was placed into NaX synthesis solution and hydrothermally synthesized at 100 °C oven for 7 h. The NaX synthesis solution was prepared by mixing sodium silicate, sodium aluminum, and sodium hydroxide (Sinopharm Chemical Reagent Co. Ltd.) in deionized water with a molar composition of 4.2 Na_2O : 1 Al_2O_3 : 3 SiO_2 : 200 H_2O[18]. The NaX/graphite felt was washed with deionized water to remove the extra synthesize solution, and dried overnight at 80 °C.

2.2 MFC construction and operation

The dual-chamber MFCs each consisting of the unmodified or modified anode and a bare graphite felt cathode separated by a cation exchange membrane (38.5 cm^2; Nafion117, Dupont Co.,

USA) were constructed. Each cell chamber made of plexiglass had an effective volume of 70 mL. The anode chamber was inoculated with anaerobic digester sludge. The anolyte consisted of 0.31 g/L NH_4CL, 2.452 g/L $NaH_2PO_4 \cdot H_2O$, 4.576 g/L Na_2HPO_4, 0.13 g/L KCL, and 1 g/L $C_6H_{12}O_6 \cdot H_2O$ at pH 7.0. The cathodic compartment of MFCs was filled with 40 mM ferricyanide and 50 mM phosphate buffer solution (2.452 g/L $NaH_2PO_4 \cdot H_2O$, 4.576 g/L Na_2HPO_4, 0.13 g/L KCL; pH 7.0). The MFCs were operated under a fed-batch mode at constant temperature (25 ± 0.5 °C) with a connected 1000 Ω external resistance unless otherwise specified.

2.3 Analytical techniques and calculations

The voltages generated by MFCs during the experiments were recorded with a precision multimeter and a data acquisition system (Keithley Instruments 2700, USA) at a 10 min interval. The anode and cathode in the MFCs were connected to a varying resistance box for the polarization curve tests. Stable voltages were then recorded under several resistance values. The power curves of power density against current density were plotted on basis of the polarization curve. Based on the anode area, current (I) was calculated as U = IR and power (P) was computed as P = IU, where U was the voltage and R was the external resistance. Internal resistance was calculated through the polarization slope method [19]. Coulombic efficiency (CE, c%), defined as the ratio of the actual charge to the theoretical charge if the substrate was completely converted to electricity, was calculated based on a reported equation [19]. Cyclic voltammetry (CV) was performed using a CHI660D potentiostat (Shanghai Chenhua Instruments Co., Ltd.) with a three-electrode arrangement. The working electrode was connected to the cathode at a scan rate of 5 mV/s from–600 to + 600 mV (VS.SCE).

The morphology of the electrode surface was investigated with a Hitachi S-4800 scanning electron microscope (SEM). Contact-angle on the anode electrode was measured with an SL200B contact angle meter (Shanghai Solon Information Technology Co., Ltd.). Fourier transform infrared (FT-IR) spectra were recorded with a NEXUS 670 FT-IR spectrometer (NICOLET) with KBr (mass ratio of 1:10) at wave number of 4000 to 400 cm^{-1}.

At the end of each experiment, the anode electrode was removed from the MFC and dipped into 5 mL of deionized water for ultrasonic treatment (100 W, 30 min). When the biomass loaded on the anode electrode was ultrasonically suspended in water, the supernatant was separated from the solution by centrifugation at 2000 r/min for 2 min. Afterward, 0.5 mL of the supernatant was mixed with 0.5 mL of 0.1 mol/L NaOH solution. The mixture was boiled for 20 min to clear the sample. Finally, the biomass protein was determined by a modified Lowry method [20].

3. RESULTS AND DISCUSSION

3.1 Growth of zeolite NaX on graphite felt

Figure 1a shows the X-ray diffraction (XRD) patterns of graphite felt after modification by HNO_3-NaX or zeolite NaX. Apparently, both the modified graphite felt and the powders display XRD

peaks ascribed to zeolite X [21]. Figure 1b shows the FT-IR spectra of bare, HNO_3-pretreated and HNO_3-NaX-modified graphite felt. The absorption bands within 1100 - 1500 cm^{-1} in the graphite felt after acid treatment are less than the bare graphite felt, where the peaks represent the groups of organic binders such as polyacrylonitrile groups in graphite mats, indicating the organic matter in the graphite felt is reduced after acid treatment [22]. Three sharp peaks characteristic of the NaX anode at 460, 560 and 1090 cm^{-1} correspond to the T-O bending mode, the double six-rings as dominating secondary building unit in the NaX zeolite structure, and the asymmetric vibration of T-O-T (T=Al or Si), respectively [21]. In conclusion, NaX zeolite was successfully attached to the graphite felt surface. The bare graphite felt (1.670 g, 5.0 × 5.0 × 0.5 cm^3) is constitute of irregularly-crossed tubular smooth graphite fibers in diameter of about 20 μm (Fig. 1c). After modification by zeolite NaX, the weight of the graphite felt was 1.700 g. Very few particles were observed on the surface of the graphite fiber (Fig. 1d). More particles gathered on the surface of the graphite felt modified with 10 wt% HNO_3 solution and zeolite NaX (Fig. 1e). The weight of graphite felt (1.796 g) was higher than that of the untreated graphite felt, indicating more NaX crystals grew after acid treatment.

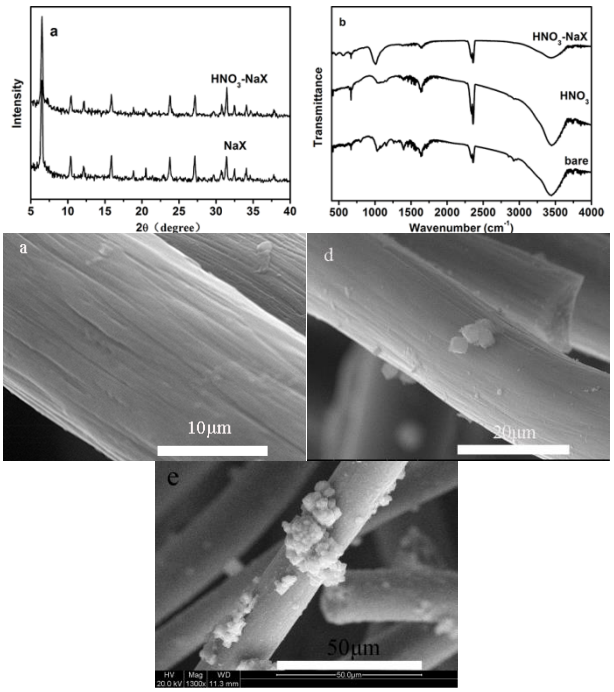

Figure 1. (a) XRD patterns and (b) FT-IR spectra of graphite felt modified by zeolite NaX or HNO_3-NaX. SEM images of (c) bare, (d) NaX-modified and (e) HNO_3-NaX-modified graphite felt.

To investigate the effect of the type of zeolite on MFC, we loaded zeolite NaA, NaX and their mixture on the graphite felt by adjusting the Si/Al molar ratio in the synthesis solution. The XRD patterns show NaA (Si/Al molar ratio of around 1), NaA-NaX mixture (Si/Al molar ratio between 1.1-2) and NaX (Si/Al molar ratio larger than 2) were successfully prepared onto the graphite felt separately (Fig. 2a) [23]. Cubic crystals with their particle size of 1-2 μm were dispersively loaded on graphite felt (Fig.

2b), which was ascribed to the NaA morphology [23]. Cubic crystals and other powders irregularly appeared on the graphite felt surface (Fig. 2c). Octahedral crystals in particle size of 3 μm gathered on the graphite felt (Fig. 2d), which was ascribed to NaX morphology. The above results indicate certain types of zeolite grew on graphite felt.

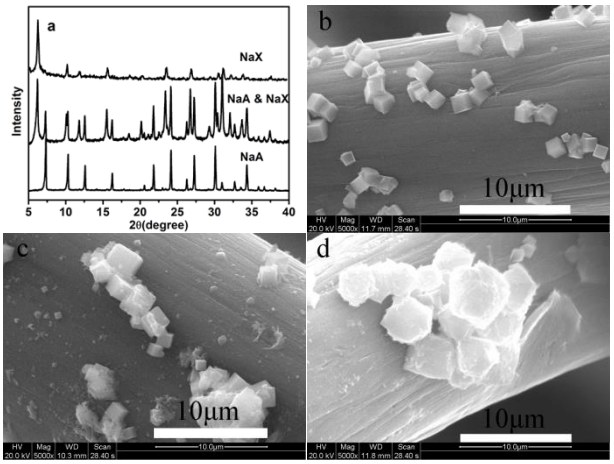

Figure 2. (a) XRD patterns and (b-d) SEM images of graphite felt when (b) NaA, (c) NaA and NaX, and (d) NaX was loaded on graphite felt surface.

To investigate the effect of zeolite weight on the graphite felt, we changed the H_2O/Al_2O_3 molar ratio in the NaX zeolite synthesis solution to 150, 250 or 500. The modified graphite felts were all crystallized for 3 h at 100 ^oC. After that, the increased weight of the three types of graphite felt were 0.285, 0.184 and 0.038 g (15.5%, 11.0% and 2.3%), respectively. When the H_2O/Al_2O_3 molar ratio of 150, the XRD spectra show diffraction peaks of both zeolite NaA and NaX (Fig. 3a), which reveal both NaA and NaX zeolite were prepared under this condition. While changing the H_2O/Al_2O_3 molar ratio of 250 or 500, however, the XRD peaks were only ascribed to NaX zeolite.

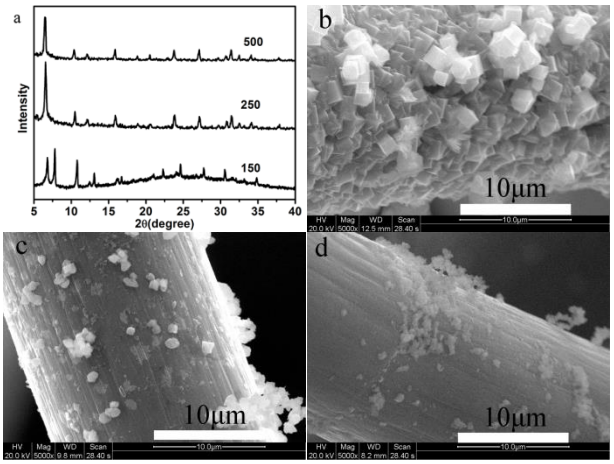

Figure 3. (a) XRD patterns and (b-d) SEM images of graphite felts at the H_2O/Al_2O_3 molar ratio of 150, 250 or 500 in the synthesis solution

3.2 MFC performance

Figure 4 shows the cell voltage curves of the three MFCs, in which the unmodified, NaX-modified or HNO_3-NaX-modified graphite felt was used as the anode separately. After inoculation, the maximum voltages (1000 Ω extra resistance) of the three MFCs with unmodified, NaX- modified and HNO_3-NaX anode were 198.9, 232.1 and 250 mV, respectively during the first feeding cycle. During the second feeding cycle, the maximum voltages of the three MFCs at similar lag time (average 0.5 d) were 528.9, 630.4 and 636.9 mV, respectively. Overall, MFCs with the NaX and HNO_3-NaX modified anodes delivered a maximum stable voltage of 609.9 and 630.4 mV, respectively, which were higher than that of MFCs with the unmodified anode (524.6 mV). These results reveal that the NaX zeolite and HNO_3 both improve the MFCs performance.

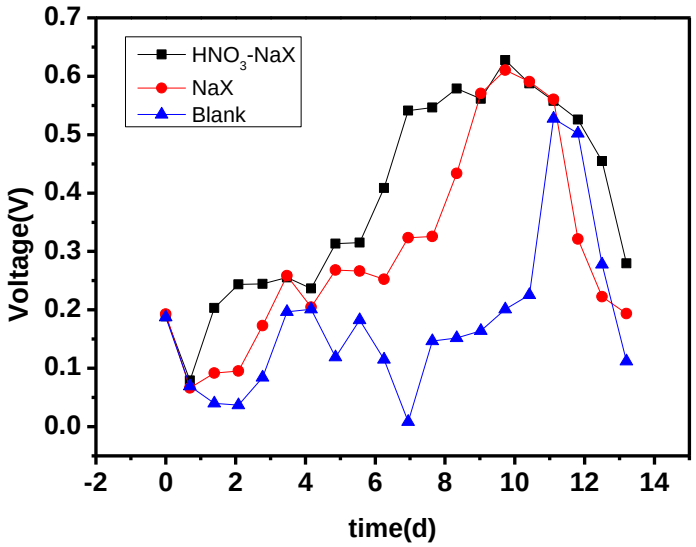

Figure 4. Voltage generation of the batch-mode MFCs with unmodified, NaX modified or HNO_3-NaX anode.

Figure 5 shows the cell voltage curves of the MFCs with different types of zeolite (NaA, NaA-NaX, NaX) and HNO_3 modified anode. The maximum voltages of the three MFCs with NaA, NaA-NaX and NaX anodes were 556.5, 628.5 and 658.0 mV, respectively. The results indicate the NaX zeolite-modified MFCs show higher output voltage than that of the NaA zeolite-modified MFC. Though zeolite NaA and NaX have similar molar ratio of Si/Al and pore size, their molecule structure are 8 O-rings and 10 O-rings, respectively, resulting in a difference in MFCs [23].

Figure 6 shows the cell voltage curves of the MFCs with different amounts of zeolite-modified anode. The H_2O/Al_2O_3 molar ratio in the NaX zeolite synthesis solution changed to 150, 250 or 500, and the weights of the three anodes gained by 0.285, 0.184 and 0.038 g, respectively. The maximum voltages of the three MFCs were 608.7, 658.7 and 599.2 mV, respectively. Moreover, the sustainable periods near the maximum voltages of MFCs were 1.1, 3.2, and 2.6 d, respectively. The above results indicate the MFCs ought to be prepared at the H_2O/Al_2O_3 molar ratio around 250.

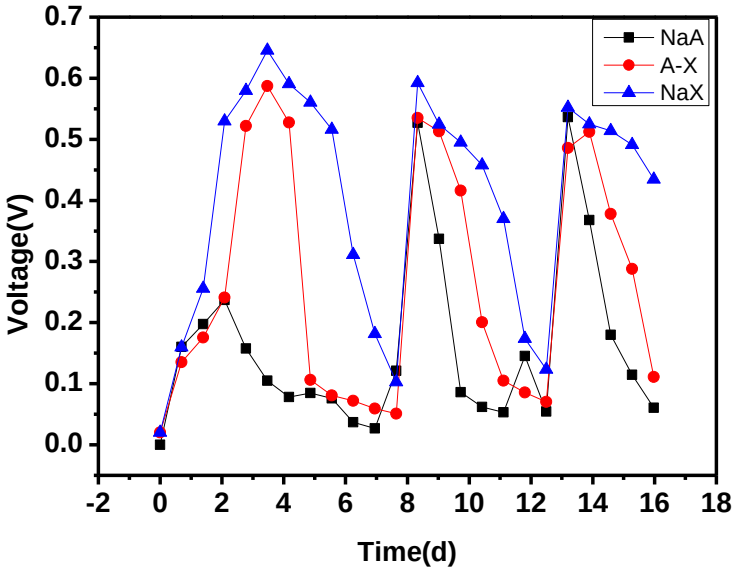

Figure 5. Voltage generation of the batch-mode MFCs with NaA, NaA-NaX and NaX anode.

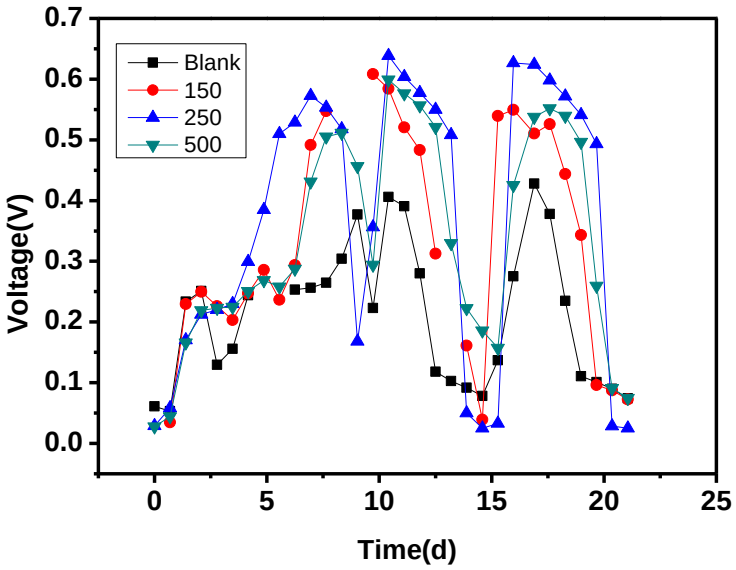

Figure 6. Voltage generation of the batch-mode MFCs with anode modified with NaX zeolite at the H_2O/Al_2O_3 molar ratio of 150, 250, 500, respectively.

3.3 Mechanism of zeolite in MFC and its performance

In conclusion, the MFC performance is greatly improved by modifying the anode with zeolite (Fig. 4), which may be related to the effective transfer of electrons released from the microbes to the external circuit via the anode. The wettability of the electrode surface significantly affects the electron transfer efficiency [24]. The hydrophilic oxygen-containing functional group on the anode surface of MFCs acts as a mediator to accelerate the electron transfer to the graphite anode [25]. Measurements

show the contact angle of the bare graphite felt is 126.2° (Fig. 7a), while that of the NaX-modified graphite felt is almost 0 (Fig. 10b), which indicates the super-hydrophilicity of the NaX-modified graphite surface. The above results reveal the enhanced wettability of graphite leads to the improved MFC performance.

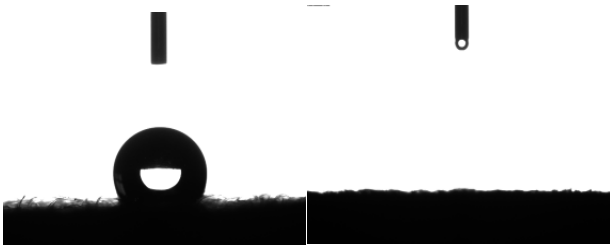

Figure 7. Images of contact angle of (a) bare and (b) NaX-modified graphite felt.

Moreover, the enhanced wettability may affect the bacteria adsorption on the anode surface. Figure 8a to c shows the biofilms of three anodes after 14 d of operation. The bacterial cells in Fig. 8b and c noticeably increased in number compared to Fig. 8 a. Bacterial cells were connected to other in a chain, and the catenular cells gathered near the NaX zeolite (Fig. 8b). Figure 8c displays almost full coverage of catenular bacterial cells, and more zeolite crystals were observed. This phenomenon may be due to the adsorption of glucose molecules in cell chamber by hydrophilic and microporous NaX zeolite particles on the anode, which attached more bacterial cells. Based on Ching's article, glucose can be adsorbed and diffused in NaX pore channel [26]. Other organic molecular, such as glycerol, gasoline, ammonia, could also effectively absorbed by NaX zeolite according to recent research [27-29]. Figure 9 displays the adsorption behavior of NaX zeolite to glucose molecules. In the experiments, 0.1 g of NaX zeolite and 50 mL of 0.1 g/L glucose were mixed under stirring. The glucose concentration was tested at 4, 8, 12, 16, 20 ,24, 28, 32 and 48 h. The adsorption amount of glucose decreased by almost 50% at 20 h. This result reveals the enhanced glucose adsorption ability enables the NaX-modified anode to attach more bacterial cells.

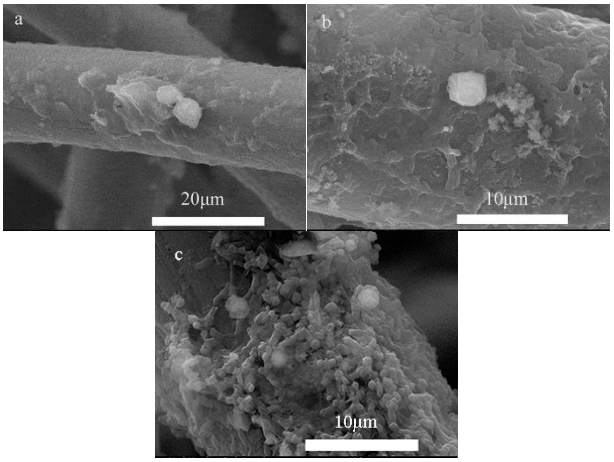

Figure 8. SEM images of biofilms on (a) bare, (b) NaX-modified and (c) HNO_3-NaX-modified anode after 14 d of operation

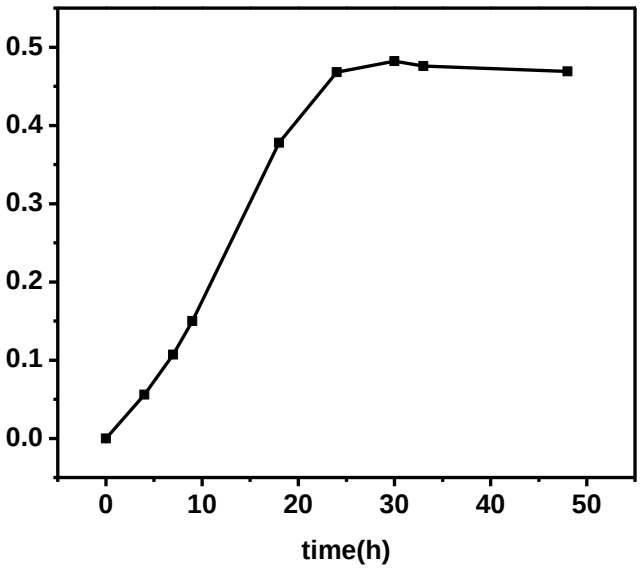

Figure 9. Adsorption curve of 0.1 g of NaX zeolite to 50 mL of 0.1 g/L glucose solution.

To investigate the influence of NaX zeolite on bacterial adhesion, we examined the total protein amounts of the bare, glucose-modified, NaX-modified and glucose-NaX-modified graphite felt (denoted as S-0, S-1, S-2, S-3 respectively) immersed in anaerobic digester sludge for 14 h. The bacteria concentrations centrifuged from four graphite anodes were 6.44, 8.61, 14.98 and 20.41 μg/ml respectively (Table 1). And the total protein amounts were 1277.38, 1789.56, 3112.76, and 4242.33 μg respectively. The above results indicate the bacterial bacterial adsorption ability can be improved by glucose and NaX modification. The NaX zeolite shows a better bacterial bacterial adsorption ability than the glucose, while the S-3 exhibits the best bacterial adsorption ability.

Table 1. Concentration and total amount of proteins of S-0, S-1, S-2, S-3.

	S-0	S-1	S-2	S-3
Concentration (μg/ml)	6.4372	8.6114	14.9787	20.4142
Total amount of proteins (μg)	1277.38	1789.56	3112.76	4242.33

Figure 10 displays the SEM images of graphite felt at the H_2O/Al_2O_3 molar ratio of 150, 250 and 500 in the synthesis solution. Clearly, many crystals were loaded on the graphite felt, but the bacterial cells can be hardly observed (Fig. 10a). A few crystals were dispersed on the graphite felt in Fig. 10 b, and the surface was almost fully covered by bacterial cells connected in a chain. Only some irregularly-shaped particles were dispersed on the graphite felt, and the cells were also hardly observed (Fig. 10c). These phenomenon show that the surface energy is decreased after the agglomeration of zeolite crystals, which is not benefit for bacterial adhesion, which is consistent with Belaabed's article [30]. In

conclusion, more zeolites can enhance the bacterial adsorption ability of graphite felt, but large amount of agglomerated crystals cannot provide suitable environment for microbial growth.

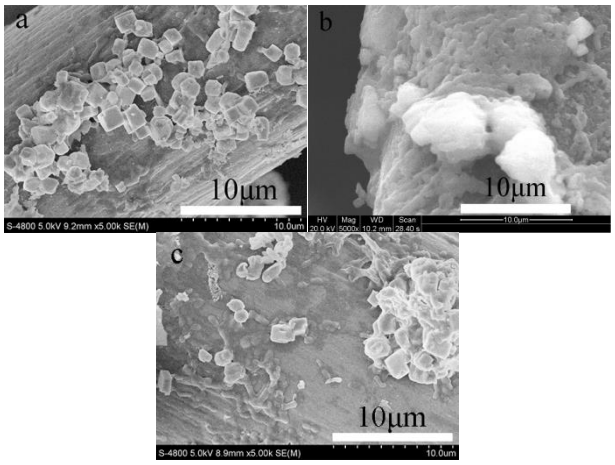

Figure 10. SEM images of biofilms of the graphite felts at the H_2O/Al_2O_3 molar ratio of 150, 250 or 500 in the synthesis solution after 14 d of operation.

4. CONCLUSIONS

Zeolite-modified graphite anode was prepared by an in-situ hydrothermal method combined with acid pre-treatment, and it showed higher output voltage in the dual-chamber microbial fuel cells (MFCs) compared with bare graphite felt anode. The NaX-zeolite-modified MFC outperformed the NaA-zeolite-modified anode. Dispersion of more zeolite on the graphite felt can improve the MFC performance. The effects of zeolite on bacterial adsorption were examined. The wetting and glucose adsorption abilities of the anode were greatly improved by zeolite modification and enabled the anode to attach more bacterial cells.

ACKNOWLEDGEMENT
We are grateful for financial support from the Key University Science Research Project of Jiangsu Province (16KJA430007), Opening Topic of Key Laboratory of Attapulgite Resources Utilization in Jiangsu Province (HPK201804) and Opening Topic of National Local Joint Engineering Research Center for Deep Utilization of Mineral and Salt Resources (SF201804).

References

1. X. Wu, F. Tong, T. Song, X. Gao, J. Xie, C. Zhou, L. Zhang, P. Wei, *J. Chem. Tech. Biotech.*, 90 (2015) 87.
2. I. Gajda, J. Greenman, C. Santoro, A. Selov, C. Melhuish, P. Atanassov, L. Leropoulos, *Energy*, 144 (2018) 1073.

3. S. Li, C. Cheng, A. Thomas, *Adv. Mater.*, 29 (2017) 179.
4. N. Eaktasang, C. Kang, H. Lim, O. Kwean, S. Cho, Y. Kim, H. Kim, *Bioresour. Technol.*, 210 (2016) 61.
5. J. Madjarov, A. Götze, R. Zengerle, S. Kerzenmarcher, *Bioresour. Technol.*, 257 (2018) 274.
6. B. Kim, J. An, *Chemsuschem*, 10 (2017) 612.
7. Z. Huang, A. Gong, D. Hou, L. Hu, Z. Ren, *Environ. Sci-Wat. Res.*, 3 (2017) 940.
8. Y. J. Feng, Q. Yang, X. Wang, B. E. Logan, *J. Power Sources*, 195 (2010) 1841.
9. K. Suzuki, Y. Kato, A. Yui, S. Yamanoto, S. Ando, O. Rubaba, Y. Tashiro, H. Futamata, *J. Biosci. Bioeng.*, 125 (2018) 565.
10. P. Zhang, J. Liu, Y. Qu, J. Zhang, Y. Zhong, Y. Feng, *J. Power Sources*, 361 (2017) 318.
11. B. T. Li, J. Zhou, X. X. Zhou, B. K. Li, C. Santoro, M. Grattieri, S. Babanova, K. Artyushkova, P. Atanassov, A. J. Schuler, *Electrochim Acta*, 134 (2014) 116.
12. Y. Wang, Q. Wen, Y. Chen, J. Yin, T. Duan, *Appl. Biochem. Biotech.*, 180 (2016), 1372.
13. W. Huang, J. Chen, Y. Hu, J. Chen, J. Sun, L. Zhang, *Int. J. Hydrogen Energy*, 42 (2016) 2349.
14. R. Umaz, C. Garrett, F. Qian, B. Li, L. Wang, *IEEE T. Power Electr.*, 32 (2016) 1.
15. P. Dugkhuntod, C. Wattanakit, *Catalysts*, 10 (2020) 245.
16. S. M. Auerbach, K. A. Carrado, P. K. Dutta, Handbook of zeolite science and technology, CRC press (2003).
17. A. C. Bose, Inorganic membranes for energy and environmental applications, Springer (2009).
18. X. Y. Wu, F. Tong, X. Y. Yong, J. Zhou, L. X. Zhang, H. H. Jia, P. Wei, *J. Hazards Mater.*, 308 (2016) 303.
19. B. E. Logan, B. Hamelers, R. Rozendal, et al, *Environ. Sci. Tech.,* 40 (2006) 5181.
20. B. Frolund, T. Griebe, P. H. Nielsen, *Appl. Microbiol Biotech.,* 43 (1995) 755.
21. M. Ansari, A. Aroujalian, A. Raisi, B. Dabir, M. Fathizadeh, *Adv. Powder Tech.*, 25 (2014) 722.
22. Z. Zhang, J. Xi, H. Zhou, X. Qiu, *Electrochim. Acta*, 218 (2016) 15.
23. S. Azizi, S Ghasemi, M. Mikhchian, *RSC Adv.*, 6 (2016) 52058.
24. M. Dozzi, S. Marzorati, M. Longhi, M. Coduri, L. Artiglia, E. Selli, *Appl. Catal. B-Environ.*, 186 (2016) 157.
25. X. Mei, D. Xing, Y. Yang, Q. Liu, H. Zhou, C. Guo, N. Ren, *Bioelectrochemistry*, 117 (2017) 29.
26. C. Ching, D. Ruthven, *Zeolites*, 8 (1988) 68.
27. Y. Lin, B. Lo, Q. Jin, I. Wilkinson, T. Hughes, C. Murray, C. Tang, S. Tsang, *Chem. Commun.*, 52 (2016) 3422.
28. P. Pietrzyk, K. Góra-Marek, *Phys. Chem. Chem. Phys.*, 18 (2016) 9490.
29. M. Mohideen, Y. Belmabkhout, P. Bhatt, A. Shkurenko, Z. Chen, K. Adil, M. Eddaoudi, *Chem. Commun.*, 54 (2018) 9414.
30. R. Belaabed, S. Elabed, A. Addaou, A. Laajab, M. Rodriguez, A. Lahsini, *Bol. Soc. Esp. Ceram. V.*, 55 (2016) 152.